ACS OMEGA

http://pubs.acs.org/journal/acsodf

Article

Foaming of Poly(3-hydroxybutyrate-*co*-3-hydroxyvalerate) with Supercritical Carbon Dioxide: Foaming Performance and Crystallization Behavior

Jin-Ke Xu, Li Zhang,* De-Long Li, Jin-Biao Bao, and Zong-Bao Wang

Cite This: *ACS Omega* 2020, 5, 9839−9845

Read Online

ACCESS | Metrics & More | Article Recommendations

ABSTRACT: Poly(3-hydroxybutyrate-*co*-3-hydroxyvalerate) (PHBV) samples were successfully foamed using supercritical carbon dioxide as a physical foaming agent. PHBV sheets were first saturated at 175 °C followed by a foaming process at different temperatures (145 to 165 °C) and different CO_2 pressures (10 to 29 MPa). It was found that microcellular structures with average cell sizes ranging from 6 to 22 μm and cell densities ranging from 10^8 to 1.2 × 10^9 cells/cm^3 could be controllably prepared by selecting suitable foaming conditions. To investigate crystallization behavior during the foaming process and explore the corresponding foaming mechanism, differential scanning calorimetry, wide angle X-ray diffraction, and small-angle X-ray scattering characterizations were carried out. Stretching behavior during the cell growth stage may increase the crystal nucleation rate, and the generated crystal nucleus accelerates the crystallization rate as well as thickens PHBV crystal lamellae.

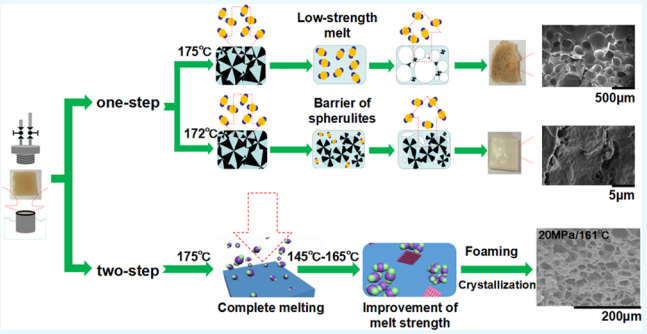

1. INTRODUCTION

The demands of environmental protection and sustainable development have given rise to the need for novel biodegradable polymers. Among which, poly(3-hydroxybutyrate-*co*-3-hydroxyvalerate) (PHBV) is one of the most attractive candidates. PHBV has a better oxygen barrier property than poly(ethylene terephthalate) (PET) and much better water vapor resistance than polylactic acid (PLA).[1,2] Along with superior degradability, biocompatibility, piezoelectricity, and mechanical performances, PHBV is expected to be applied as scaffold materials, drug release agents, and electronic materials.[3−6]

Light weight and low cost are extremely important for exploiting the practical applications of biodegradable polymers. One key strategy is to construct cellular morphology in the polymer matrix. Over the past 10 years, supercritical carbon dioxide ($scCO_2$) has received considerable attention as a foaming agent for polymeric foams[7−32] owing to its nontoxicity and nonflammability.[15−17] It is well known that the foaming behavior of semicrystalline polymers is much more complicated than that of amorphous polymers on account of the existence of crystals.[17] The existing crystal regions not only decrease the CO_2 solubility in the matrix but also influence cell nucleation and cell growth. In the nucleation step, the interface between crystal phases and amorphous phase is beneficial for CO_2 accumulation, which leads to less Gibbs free energy needed for nucleating at the interface than that necessary for homogeneous nucleation. Meanwhile, in the cell growth step, the formed cells are constrained by the crystal region owing to its stiffness.[17−19] Among the semicrystalline polymers, PLA foaming behavior under compressed CO_2 has been extensively discussed.[12,13,17−20] Yang et al.[20] investigated the effect of crystallinity and crystalline morphology on the cell structure and found that both played an important role in the cell structure. The ring banded spherulite induced by compressed CO_2 in the temperature range of 90−110 °C facilitated to prepare uniform PLA foam. Xu and Huang[17] discussed the influence of crystallinity and spherulite size on the cell structure and expansion ratio. Voiding formation of spherulites during the foaming process is vital for preparing a uniform cell structure.

However, there is a lack of research on the preparation of PHBV foam. Only a few works have reported them by the extrusion foaming process. Le Moigne et al.[22] prepared PHBV/organoclay composite foams with 50% porosity by a $scCO_2$-assisted extrusion foaming method. They showed that the crystallization of PHBV during the foaming process hampered

Received: December 31, 2019
Accepted: April 13, 2020
Published: April 22, 2020

https://dx.doi.org/10.1021/acsomega.9b04501
ACS Omega 2020, 5, 9839−9845

the CO_2 diffusion within the PHBV matrix and hence restricted growth of pores. Szegda et al.[23] reported extrusion foaming of PHBV foams with the aid of a chemical blowing agent. The density of extruded foams reduced up to about 60% compared to pure PHBV. However, no literature has reported the successful preparation of PHBV foam with uniform cell size and high cell density to the best of our knowledge. The extrusion foaming process of PHBV[22,23] can certainly melt the total crystalline region and avoid the drawbacks raised by them. Nevertheless, the melt strength is too weak to prevent the formed cells from collapse and coalescence due to the linear chain structure of the PHBV molecule. Therefore, the corresponding PHBV products have uneven cell size distributions and low expansion ratios.

PHBV is difficult to melt completely even when heated to its melting temperature (172 °C, DSC data) owing to its large size of spherulites and high crystallinity up to 60%. On the other hand, when heated at a sufficiently high temperature (i.e., 175 °C) to melt the crystalline region, PHBV's low melt strength and less CO_2 dissolution in the polymer matrix impede the foamability of PHBV[27]. In this work, the PHBV foams with uniform cell size and high cell density were prepared using the $scCO_2$-assisted batch foaming process. We assess the influence of foaming parameters such as foaming temperature, saturation pressure, etc., on the cellular morphology of PHBV foams and discuss crystallization behavior during the foaming process.

2. RESULTS AND DISCUSSION

2.1. Exploration of the PHBV Foaming Strategy. At first, a one-step PHBV foaming process in the foaming temperature range of 160−178 °C with 20 MPa was carried out. When the foaming temperature was lower than 172 °C, the obtained PHBV samples showed almost no expansion compared to the original samples, but the sample color turned from yellowish brown to white. For the case of 172 °C, the cross-sectional morphology of PHBV foam showed no internal microcellular structure (see Figure 1a). However, much smaller

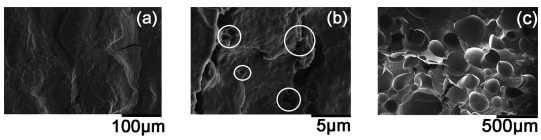

Figure 1. Cell morphologies of foamed PHBV at various foaming temperatures: (a,b) 172 °C; (c) 175 °C.

pores with sizes less than 1 μm were observed (marked by white circles in Figure 1b). This indicates that high stiffness strongly limits cell growth. According to EL-Hadi et al.,[33] crystalline regions in PHBV are composed of large spherulites, which could not melt when the temperature is not high enough. This prevents CO_2 from dissolving into the polymer melt and restricts cell growth.[34] When the foaming temperature is 175 °C, higher than its melting point of 172 °C, cells tend to grow and undergo coalescence, leading to big pores even larger than 5 mm (see Figure 1c). According to Le Moigne et al.[22] and Szegda et al.,[23] PHBV has relatively low melt strength above its melting point, which would induce the escape of a large amount of CO_2 from the melt and the collapse and coalescence of cells. This issue poses serious challenge to the PHBV foaming process.

Consequently, no foaming windows can be found in one-step foaming technology. To overcome the high crystallinity barrier and low melt strength challenge, a two-step foaming process was developed in this work. For this two-step foaming process, PHBV samples were first saturated at 175 °C for 30 min to completely melt the crystalline regions. This step aimed at facilitating dissolution of $scCO_2$ into the PHBV matrix. Subsequently, the sample was cooled down to the foaming temperate in the range of 145−165 °C to improve melt strength. Finally, the valve was open to release the compressed CO_2 rapidly. Cell growth at the initial depressurization stage accelerates the crystal nucleation rate and generates more crystal nuclei, which favors the improvement of melt strength.

2.2. Effect of the Foaming Temperature. Typical SEM images of foaming PHBV obtained under 20 MPa at various foaming temperatures are shown in Figure 2. For the case of

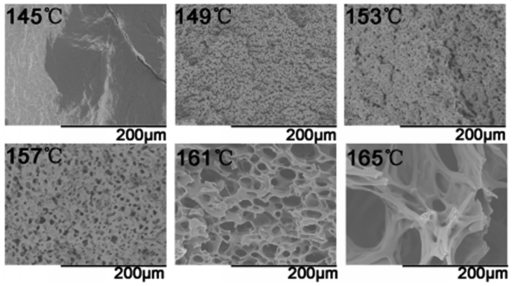

Figure 2. Cell morphologies of PHBV foamed at different temperatures under 20 MPa.

145 °C, almost no microcellular morphology is observed. When the temperature increases to 149 °C, legible cell structures with thick cell walls are obtained. Further increasing the temperature to 154−161 °C induces thinner cell walls and partially connected cells. Especially at 161 °C, some open-cell structures are obtained, which indicates that the melt strength gets weaker, and the rupture of the cell walls initiates at this temperature. When the foaming temperature further increases to 165 °C, the melt strength is insufficient to support cell growth, leading to cell collapse and coalescence.[16]

Figure 3 shows that the relative density and cell density decrease with increasing temperature, while the average cell size increases. This is because the solubility of CO_2 in the PHBV matrix decreases as the foaming temperature increases.[28] The number of nucleation sites decreases with the reduction of CO_2 concentration in the PHBV matrix. In

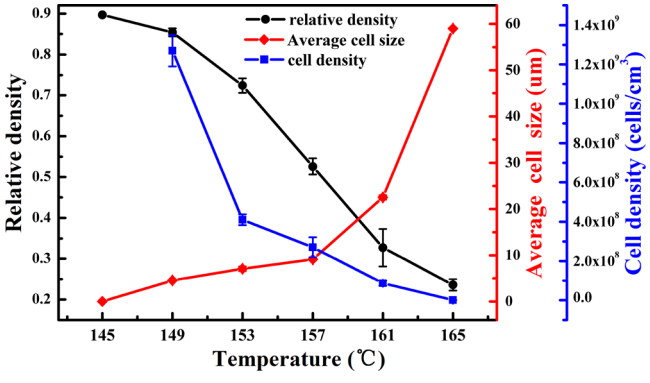

Figure 3. Effects of foaming temperatures on the cell morphology of PHBV foams.

https://dx.doi.org/10.1021/acsomega.9b04501
ACS Omega 2020, 5, 9839−9845

addition, the melt strength weakens at higher foaming temperature, which leads to fast growth and rupture of the cells. PHBV foams with cell sizes in the range of 6 to 22 μm and cell densities in the range of 10^8 to 1.2×10^9 cells/cm^3 could be obtained by selecting suitable foaming temperature under a pressure of 20 MPa.

2.3. Effect of the Saturation Pressure. Figure 4 shows the SEM images of PHBV foam at 161 °C under different

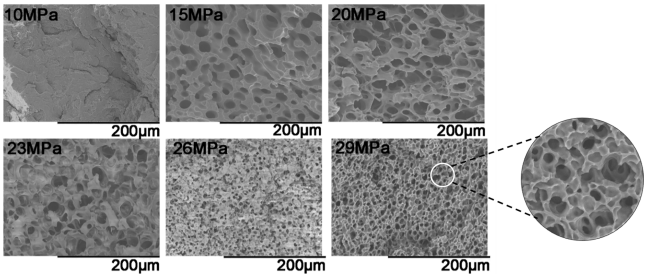

Figure 4. Cell morphologies of PHBV foamed under different saturation pressures at 161 °C.

saturation pressures. At this temperature, microcellular structures appear under 15 MPa. As the pressure increases to 20 MPa, the cell size increases, and the cell walls get thinner. Under saturation pressures of 23−29 MPa, the average cell size decreases with increasing pressure, while more open-cell structures are observed. As shown in Figure 5, when the

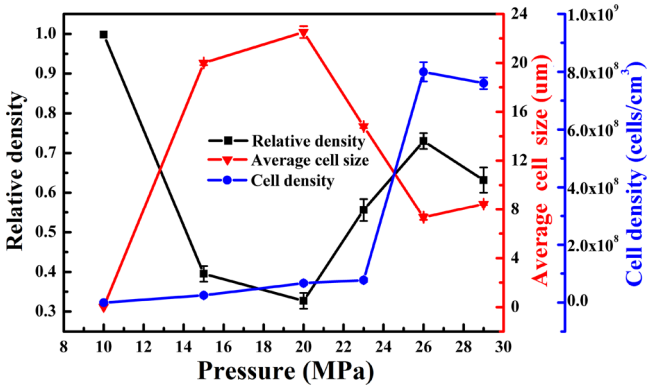

Figure 5. Effects of saturation pressure on the cell morphology of PHBV foams.

saturation pressure is in the range of 10−20 MPa, the average cell size increased from 0 to 23 μm, and the cell density increased to 9.5×10^7 cells/cm^3. This is attributed to the increase of CO_2 solubility in the PHBV matrix with increasing pressure. CO_2 molecules reduce the melt strength by plasticizing the molecule mobility through swelling, which makes cells grow more easily. However, when the saturation pressure is in the range of 23−29 MPa, the average cell size reduces from 23 to 8 μm, and the cell density increases from 1×10^8 to 8×10^8 cells/cm^3. This is because the increase of the CO_2 adsorption level in the matrix reduces the energy barrier of nucleation and increases the nucleation density.[14] Therefore, the cell walls get thinner, and the open-cell structures increase (see white circles in Figure 4).

2.4. Crystallization Behavior of PHBV and PHBV Foams. As reported previously, the foaming process is usually accompanied by a change of crystallization behavior,[35] which would directly influence the melt strength and foamability of PHBV. The crystallization behavior of PHBV was investigated via DSC. As shown in Figure 6, all PHBV foams exhibit double

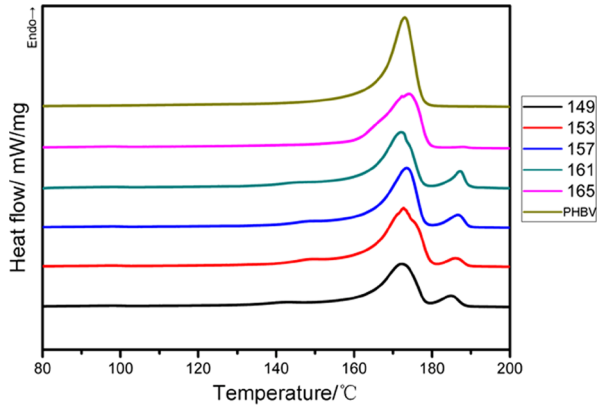

Figure 6. DSC curves of PHBV foamed at different temperatures under 20 MPa.

melting peaks (T_{m1} and T_{m2}), whereas unfoamed PHBV shows a single melting point (T_{m1}). This demonstrates that the CO_2 molecules take part in the foaming process and affect the crystallization behavior of PHBV foams.

For the process here, the PHBV sheet was first controlled at a saturation temperature of 175 °C to completely melt the crystalline region during the saturation stage, then cooled down to the foaming temperature in the range of 145−165 °C, and finally subjected to nucleation and cell growth by reducing pressure. Szegda et al.[23] reported that the crystallization temperature of PHBV is around 125 °C, which is much lower than both the saturation and foaming temperatures herein. Moreover, the plasticization effect of CO_2 molecules tends to postpone the crystallization peak to a lower temperature region.[17,18,26] These reasons make PHBV difficult to crystallize in the saturation and foaming stages before releasing pressure. Therefore, the crystallization of foamed PHBV occurred in the stage of cell growth; that is, the cell growth would stretch the melt and affect the crystallization behavior. T_{m1} for both foamed and unfoamed PHBV is located at 173 °C, which indicates the formation of a similar crystalline structure. Interestingly, T_{m2} of foamed PHBV in the range of 186−188 °C increases with the increase of foaming temperature. This reflects that perfect crystals or new crystalline phases may be formed at higher foaming temperature with the lubricating CO_2 molecules dissolved in the PHBV matrix.[36]

We further implemented WAXD and SAXS measurements to investigate the change in crystalline structures. The WAXD curves of the PHBV foams prepared at different temperatures under a pressure of 20 MPa are shown in Figure 7. The peaks shown in diffraction curves at around 13.7, 17.2, 20.3, 21.8, 22.7, 25.9, and 27.5° correspond to the (020), (110), (021), (101), (111), (121), and (040) diffraction planes of PHBV.[37] Phongtamrug and Tashiro[38] reported that high tension in PHBV processing induces new crystalline phases, attributed to the α-to-β structural change in both amorphous and crystalline regions, while the β-form peaks appear around the (110) diffraction plane. However, no new peaks around the (110) diffraction plane were observed in this work, which indicates that no new crystalline phases were generated during the foaming process. From the WAXD data, it can be found that

https://dx.doi.org/10.1021/acsomega.9b04501
ACS Omega 2020, 5, 9839−9845

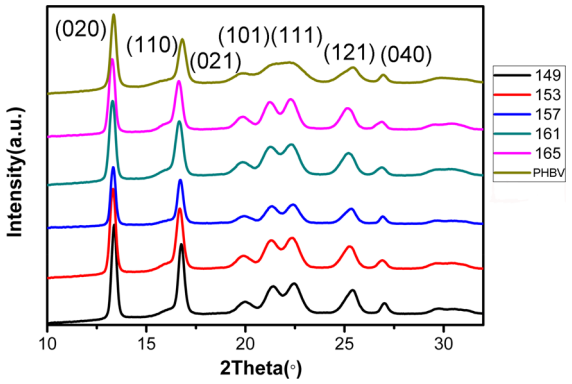

Figure 7. WAXD curves of PHBV foamed at different temperatures under 20 MPa.

the crystallinity of the foamed PHBV is higher than that of the unfoamed one (Table 1). The SAXS curves of the PHBV foam

Table 1. Parameters Calculated from WAXD and SAXS Curves of PHBV Samples

foaming temperature (°C)	saturation pressure (MPa)	crystallinity (%)	long spacing (nm)	lamellar thickness (nm)
149	20	63.50	8.60	5.47
153	20	68.32	9.34	6.38
157	20	70.30	8.75	6.15
161	20	67.30	8.85	5.96
165	20	67.12	10.50	7.05
neat PHBV	0	59.72	6.56	3.92

calculated from Lorentz-corrected plots are shown in Table 1. It can be seen in Figure 8 that the q value of the PHBV foam is

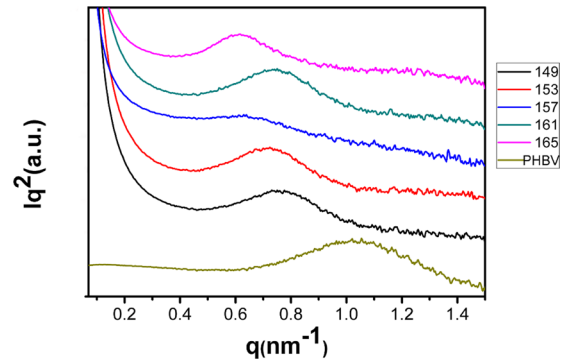

Figure 8. SAXS curves of PHBV foamed at different temperatures under 20 MPa.

lower than that of the unfoamed one, indicating that the PHBV foam has a higher long period spacing; the crystal lamellae of PHBV may get thicker in the foaming process. Actually, the foaming behavior may reduce the crystal nucleation energy barrier and accelerate the crystallization rate, similar to the effect of biaxial stretching.[27] As a result, the generated crystal nucleus acting as heterogeneous nucleation may thicken PHBV crystal lamellae to withstand the growth of cells at the initial depressurization. Therefore, the stretching process of cell growth may thicken the crystal lamella, causing double melting peaks of PHBV foams (see Figure 6).

3. CONCLUSIONS

The foamed PHBV samples were prepared using $scCO_2$ as the physical foaming agent. The effects of foaming temperature and saturation pressure on cell morphology were discussed. It was found that the microcellular structures with average cell sizes ranging from 6 to 22 μm and cell densities ranging from 10^8 to 1.2×10^9 cells/cm^3 could be controllably prepared by selecting suitable foaming conditions. In order to discuss the crystallization behavior during the foaming process, DSC, WAXD, and SAXS were performed. For this case, the crystallization behavior of PHBV is difficult to occur in the saturation and foaming stages before reducing the pressure, whereas it occurs in the cell growth stage. The foaming behavior may reduce the crystal nucleation energy barrier and accelerate the crystallization rate, and the generated crystal nucleus acting as heterogeneous nucleation may thicken PHBV crystal lamellae.

4. EXPERIMENTAL SECTION

4.1. Materials. ENMAT Y1000 PHBV with 3% hydroxyvalerate content was manufactured by Tianan Biologic Material Co. (Ningbo, P. R. China) in powder form with a density of 1.24 g/cm^3. TGA analysis shown in Figure 9 was

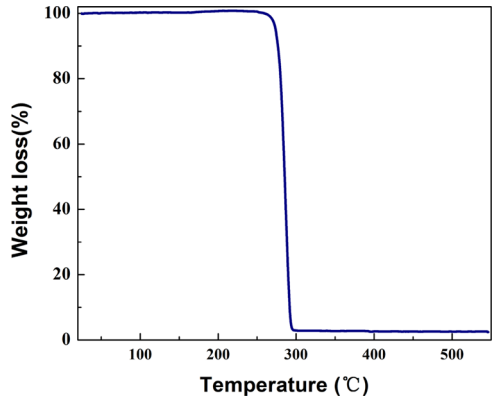

Figure 9. TGA curve of pure PHBV sample.

performed to determine the thermal stability of PHBV. The average molecular weight of the PHBV was about 300000. CO_2 with 99.95% purity was supplied by Fangxin Gas Inc. (Ningbo, P. R. China).

4.2. Sample Preparation. The PHBV powder was first dried in a vacuum oven at 60 °C for 9 h. Then PHBV sheets of 75 mm × 10 mm × 2 mm in size were prepared by a Minilab twin-screw extruder (Thermo Electron, Germany). The screw rotation speed, processing temperature, mold temperature, and injection pressure were preset at 15 rpm, 172 °C, 90 °C, and 500 bar, respectively.

4.2.1. Two-Step Foaming Process. The foaming process is shown in Figure 10. The sheets were placed in a high-pressure vessel heated in a silicone oil bath. After the vessel was swept three times with CO_2, a predetermined amount of CO_2 was charged into the vessel. The PHBV samples in the vessel were saturated with 10−20 MPa CO_2 at 175 °C for 30 min. The vessel was subsequently transferred to another silicone oil bath at foaming temperatures ranging from 145 to 165 °C and saturated for another 90 min. Thereafter, the valve was opened to release the compressed CO_2 rapidly in order to induce gas nucleation and cell growth in PHBV. When the pressure was

https://dx.doi.org/10.1021/acsomega.9b04501
ACS Omega 2020, 5, 9839−9845

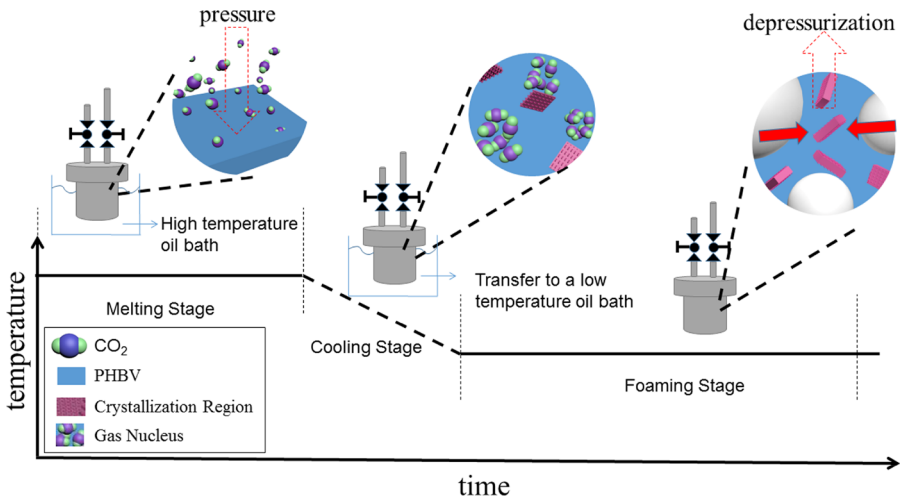

Figure 10. Schematic illustration of the two-step foaming process.

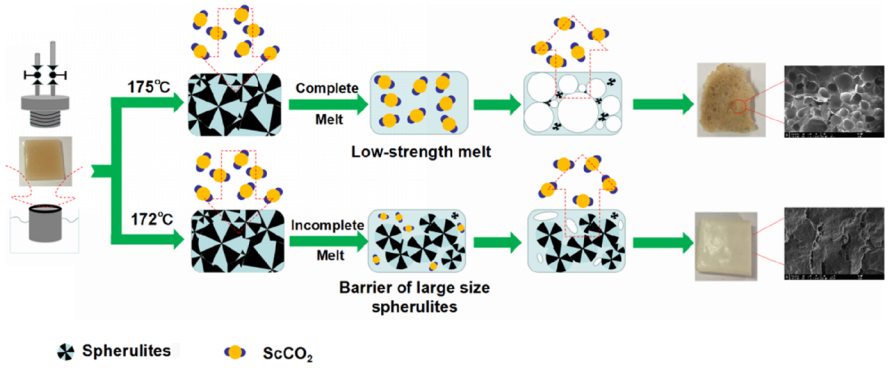

Figure 11. Schematic illustration of the one-step foaming process.

completely released, the high-pressure vessel was moved to a water-cooling system immediately, and the samples were retrieved.

For comparison, a one-step foaming process was also carried out as follows (see Figure 11). After the vessel was swept three times with CO_2, the PHBV sheets were charged into the vessel and directly heated to different foaming temperatures (160−178 °C) under the 20 MPa saturation pressure. Two hours later, the valve was opened to release the compressed CO_2 rapidly. When the pressure was completely released, the high-pressure vessel was moved to a water-cooling system immediately, and the samples were retrieved.

4.3. Characterization. Thermal properties of PHBV and PHBV foams were characterized using differential scanning calorimetry (DSC, Mettler Toledo) under a flowing nitrogen atmosphere. All specimens (5−8 mg) were heated to 200 °C with a heating rate of 10 °C/min.

The thermal stability of PHBV was measured by thermogravimetric analysis (TGA) in a TG/DTA 7300 instrument (Seiko, Chiba, Japan) from 30 to 600 °C at a heating rate of 10 °C/min under a constant nitrogen flow.

The cell structure was measured using a scanning electron microscope (SEM, TM3000) with an accelerating voltage of 15 KV. The specimens were fractured by liquid nitrogen followed by sputtering with gold.

The crystallization behaviors of PHBV foams were characterized by small-angle X-ray scattering (SAXS) and wide-angle X-ray diffraction (WAXD) (Xenocs Company, France). The X-ray wavelength was 0.154 nm. The two-dimensional (2D) WAXD patterns were recorded using a Mar CCD X-ray detector (MAR345) with a resolution of 2048 × 2048 pixels. The Fit2d software package[39] was used to carry out the WAXD data analysis.

The average cell size and cell density were analyzed from SEM images using the software Image Pro-plus. The cell density, N, defined as the number of cells per unit volume of foam, was calculated by

$$N = \left(\frac{nM^2}{A}\right)^{3/2} \quad (1)$$

where n is the number of cells in the micrograph, A is the area of the micrograph (cm^2), and M is the magnification factor. The average cell size, D, defined as the volume-averaged diameter of all the cells in the micrograph, was calculated by

$$D = \left(\frac{\sum_{i=1}^{n} d_{i=1}^{3}}{n}\right)^{1/3} \quad (2)$$

A balance equipped with a density measurement (Mettler Toledo) was used to determine the mass density of foamed PHBV. The sample was first weighed in air and then in water with a mesh metal cover to ensure complete immersion. According to ASTM 792-00, the mass density of foamed PHBV, ρ, was calculated by

https://dx.doi.org/10.1021/acsomega.9b04501
ACS Omega 2020, 5, 9839−9845

$$\rho = \frac{a}{a + w - b}\rho_{water} \quad (3)$$

where a is the mass of the sample in air, w is the mass of totally immersed net-like metal cover in water, and b is the quality of the specimen and cover completely immersed in water. The relative density of the foam, R_ρ, is defined as the ratio of the density of the foam (ρ) relative to that of the unfoamed PHBV (ρ_{pure})

$$R_\rho = \frac{\rho}{\rho_{pure}} \quad (4)$$

AUTHOR INFORMATION

Corresponding Author

Li Zhang − *Ningbo Key Laboratory of Specialty Polymers, Faculty of Materials Science and Chemical Engineering, Ningbo University, Ningbo 315211, China;* orcid.org/0000-0003-2684-0414; Email: zhangli2@nbu.edu.cn

Authors

Jin-Ke Xu − *Ningbo Key Laboratory of Specialty Polymers, Faculty of Materials Science and Chemical Engineering, Ningbo University, Ningbo 315211, China*

De-Long Li − *Ningbo Key Laboratory of Specialty Polymers, Faculty of Materials Science and Chemical Engineering, Ningbo University, Ningbo 315211, China*

Jin-Biao Bao − *Ningbo Key Laboratory of Specialty Polymers, Faculty of Materials Science and Chemical Engineering, Ningbo University, Ningbo 315211, China*

Zong-Bao Wang − *Ningbo Key Laboratory of Specialty Polymers, Faculty of Materials Science and Chemical Engineering, Ningbo University, Ningbo 315211, China*

Complete contact information is available at: https://pubs.acs.org/10.1021/acsomega.9b04501

Author Contributions

All authors contributed to the discussion and writing of the manuscript. The final version of the manuscript was approved by all authors.

Notes

The authors declare no competing financial interest.

ACKNOWLEDGMENTS

This work is financially supported by National Natural Science Foundation of China (No. 51403110), the Natural Science Foundation of Zhejiang Province (No. LY19E030003), the Natural Science Foundation of Ningbo City (No. 2019A610145), and K. C. Wong Magna Fund in Ningbo University.

REFERENCES

(1) Cava, D.; Giménez, E.; Gavara, R.; Lagaron, J. M. Comparative performance and barrier properties of biodegradable thermoplastics and nanobiocomposites versus PET for food packaging applications. *J. Plast. Film Sheeting* **2016**, *22*, 265−274.

(2) Shogren, R. Water vapor permeability of biodegradable polymers. *J. Environ. Polym. Degrad.* **1997**, *5*, 91−95.

(3) Avella, M.; Martuscelli, E.; Raimo, M. Review Properties of blends and composites based on poly(3-hydroxy)butyrate (PHB) and poly(3-hydroxybutyrate-co-3-hydroxyvalerate) (PHBV) copolymers. *J. Mater. Sci.* **2000**, *35*, 523−545.

(4) Jost, V.; Langowski, H.-C. Effect of different plasticisers on the mechanical and barrier properties of extruded cast PHBV films. *Eur. Polym. J.* **2015**, *68*, 302−312.

(5) Köse, G. T.; Korkusuz, F.; Korkusuz, P.; Purali, N.; Özkul, A.; Hasirci, V. Bone generation on PHBV matrices: an in vitro study. *Biomaterials* **2003**, *24*, 4999−5007.

(6) Yu, H.; Yan, C.; Yao, J. Fully biodegradable food packaging materials based on functionalized cellulose nanocrystals / poly (3-hydroxybutyrate-co-3-hydroxyvalerate) nanocomposites. *RSC Adv.* **2014**, *4*, 59792−59802.

(7) Yan, Z.; Liao, X.; He, G.; Li, S.; Guo, F.; Li, G. Green method to widen the foaming processing window of PLA by introducing stereocomplex crystallites. *Ind. Eng. Chem. Res.* **2019**, *58*, 21466−21475.

(8) Xu, L.-Q.; Huang, H.-X. Formation mechanism and tuning for bi-modal cell structure in polystyrene foams by synergistic effect of temperature rising and depressurization with supercritical CO_2. *J. Supercrit. Fluids* **2016**, *109*, 177−185.

(9) Li, J.; Liao, X.; Yang, Q.; Li, G. Crystal in situ induced by supercritical CO_2 as bubble nucleation sites on spherulitic PLLA foam structure controlling. *Ind. Eng. Chem. Res.* **2017**, *56*, 11111−11124.

(10) Wang, S.; Xue, S.; Ge, C.; Ren, Q.; Zhao, D.; Zhai, W. Preparation of fluorescent thermoplastic polyurethane microcellular foam films blown by supercritical CO_2. *J. Cell. Plast.* **2019**, *55*, 483−505.

(11) Li, Y.; Mi, J.; Fu, H.; Zhou, H.; Wang, X. Nanocellular Foaming Behaviors of Chain-Extended Poly(lactic acid) Induced by Isothermal Crystallization. *ACS Omega* **2019**, *4*, 12512−12523.

(12) Wang, K.; Wang, S.; Wu, F.; Pang, Y.; Zhai, W.; Zheng, W. Supercritical CO2 in controlling phase morphology of polypropylene/polystyrene blends and the corresponding mechanical properties and foamability. *Polym. Bull.* **2016**, *73*, 941−957.

(13) Xue, S.; Jia, P.; Ren, Q.; Liu, X.; Lee, R. E.; Zhai, W. Improved expansion ratio and heat resistance of microcellular poly(L-lactide) foam via in-situ formation of stereocomplex crystallites. *J. Cell. Plast.* **2016**, *54*, 103−119.

(14) Sun, J.; Xu, J.; He, Z.; Ren, H.; Wang, Y.; Zhang, L.; Bao, J.-B. Role of nano silica in supercritial CO_2 foaming of thermoplastic poly(vinyl alcohol) and its effect on cell structure and mechanical properties. *Eur. Polym. J.* **2018**, *105*, 491−499.

(15) Li, B.; Zhao, G.; Wang, G.; Zhang, L.; Hou, J.; Gong, J. A green strategy to regulate celluar structure and crystallization of poly (latic acid) foams based on pre-isothermal cold crystallization and CO_2 foaming. *Int. J. Biol. Macromol.* **2019**, *129*, 171−180.

(16) Wang, Y.; Tian, H.; Bian, Q.; Xiang, A.; Ge, X.; Liu, Q. Effect of trolamine and dibutyltindilaurate on the structure and properties of polyurethane-imide foams. *Cell. Polym.* **2015**, *34*, 119−136.

(17) Xu, L.-Q.; Huang, H.-X. Foaming of Poly(lactic acid) Using Supercritical Carbon Dioxide as Foaming Agent: Influence of Crystallinity and Spherulite Size on Cell Structure and Expansion Ratio. *Ind. Eng. Chem. Res.* **2014**, *53*, 2277−2286.

(18) Li, D.; Liu, T.; Zhao, L.; Lian, X.; Yuan, W. Foaming of poly(lactic acid) based on its nonisothermal crystallization behavior under compressed carbon dioxide. *Ind. Eng. Chem. Res.* **2011**, *50*, 1997−2007.

(19) Xu, L.-Q.; Huang, H.-X. Turning cell structure and expansion ratio of thickwalled biodegradable poly(lactic acid) foams prepared using supercritical CO_2. *J. Cell. Plast.* **2019**, *56*, 89−104.

(20) Yang, Y.; Li, X.; Zhang, Q.; Xia, C.; Chen, C.; Chen, X.; Yu, P. Foaming of poly(lactic acid) with supercritical CO_2: The combined effect of crystallinity and crystalline morphology on celluar structure. *J. Supercrit. Fluids* **2019**, *145*, 122−132.

(21) Krause, B.; Mettinkhof, R.; Van der Vegt, N. F. A.; Wessling, M. Microcelluar foaming of amorphous high-Tg polymers using carbon dioxide. *Macromolecules* **2001**, *34*, 874−884.

(22) Le Moigne, N.; Sauceau, M.; Benyakhlef, M.; Jemai, R.; Benezet, J. C.; Rodier, E.; Lopez-Cuesta, J. M.; Fages, J. Foaming of poly (3-hydroxybutyrate-co-3-hydroxyvalerate) / organo-clays nano-

https://dx.doi.org/10.1021/acsomega.9b04501
ACS Omega 2020, 5, 9839−9845

biocomposites by a continuous supercritical CO_2 assisted extrusion process. *Eur. Polym. J.* **2014**, *61*, 157−171.
(23) Szegda, D.; Duangphet, S.; Song, J.; Tarverdi, K. Extrusion foaming of PHBV. *J. Cell. Plast.* **2014**, *50*, 145−162.
(24) Wang, G.; Zhang, D.; Wan, G.; Li, B.; Zhao, G. Glass fiber reinforced PLA composite with enhanced mechanical properties, thermal behavior, and foaming ability. *Polymer* **2019**, *181*, 121803.
(25) Zhang, X.; Li, B.; Wang, X.; Li, K.; Wang, G.; Chen, J.; Park, C. B. Modification of iPP microcellular foaming behavior by thermal history control and nucleating agent at compressed CO_2. *J. Supercrit. Fluids* **2018**, *133*, 383−392.
(26) Zhang, J.; Yang, S.; Yang, X.; Xi, Z.; Zhao, L.; Cen, L.; Lu, E.; Yang, Y. Novel fabricating process for porous polyglycolic acid scaffolds by melt-foaming using supercritical carbon dioxide. *ACS Biomater. Sci. Eng.* **2018**, *4*, 694−706.
(27) Hikima, Y.; Morikawa, J.; Hashimoto, T. Wavenumber Dependence of FT-IR Image of Molecular Orientation in Banded Spherulites of Poly(3-hydroxybutyrate) and Poly($_L$-lactic acid). *Macromolecules* **2013**, *46*, 1582−1590.
(28) Zhang, R.-Z.; Chen, J.; Huang, M.-W.; Zhang, J.; Luo, G.-Q.; Wang, B.-Z.; Li, M.-J.; Shen, Q.; Zhang, L.-M. Synthesis and compressive response of microcellular foams fabricated from thermally expandable microspheres. *Chin. J. Polym. Sci.* **2019**, *37*, 279−288.
(29) Xiao, S.-P.; Huang, H.-X. Generation of nanocellular TPU/reduced graphene oxide nanocomposite foams with high cell density by manipulating viscoelasticity. *Polymer* **2019**, *183*, 121879.
(30) Bao, J.-B.; Junior, A. N.; Weng, G.-S.; Wang, J.; Fang, Y.-W.; Hu, G.-H. Tensile and impact properties of microcellular isotactic polypropylene (PP) foams obtained by supercritical carbon dioxide. *J. Supercrit. Fluids* **2016**, *111*, 63−73.
(31) Zhao, Z.; Yang, Q.; Gong, P.; Sun, H.; Wu, P.; Huang, Y.; Liao, X. Effect of process temperatures on the flow-induced crystallization of isotactic polypropylene/poly(ethylene terephthalate) blends in microinjection molding. *Ind. Eng. Chem. Res.* **2017**, *56*, 9467−9477.
(32) Bocz, K.; Molnár, B.; Marosi, G.; Ronkay, F. Preparation of Low-density microcellular foams from recycled PET modified by solid state polymerization and chain extension. *J. Polym. Environ.* **2019**, *27*, 343−351.
(33) El-Hadi, A.; Schnabel, R.; Straube, E.; Müller, G.; Henning, S. Correlation between degree of crystallinity, morphology, glass temperature, mechanical properties and biodegradation of poly (3-hydroxyalkanoate) PHAs and their blends. *Polym. Test.* **2002**, *21*, 665−674.
(34) Doroudiani, S.; Park, C. B.; Kortschot, M. T. Effect of the Crystallinity and Morphology on the Microcellular Foam Structure of Semicrystalline Polymers. *Polym. Eng. Sci.* **1996**, *36*, 2645−2662.
(35) Zhai, W.; Ko, Y.; Zhu, W.; Wong, A.; Park, C. A study of the crystallization, melting, and foaming behaviors of polylactic acid in compressed CO_2. *Int. J. Mol. Sci.* **2009**, *10*, 5381−5397.
(36) Yang, J. Origin of double melting peaks of α-form isotactic polypropylene: Recrystallization and lamellar thickness hierarchy. *J. Appl. Polym. Sci.* **2010**, *118*, 1520−1526.
(37) Zhu, H.; Lv, Y.; Duan, T.; Zhu, M.; Li, Y.; Miao, W.; Wang, Z. In-situ investigation of multiple endothermic peaks in isomorphous poly(3-hydroxybutyrate-co-3-hydroxyvalerate) with low HV content by synchrotron radiation. *Polymer* **2019**, *169*, 1−10.
(38) Phongtamrug, S.; Tashiro, K. X-ray Crystal structure analysis of poly(3-hydroxybutyrate) β-form and the proposition of a mechanism of the stress-induced α-to-β phase transition. *Macromolecules* **2019**, *52*, 2995−3009.
(39) Hammersley, A. P.; Svensson, S. O.; Thompson, A. Calibration and correction of spatial distortions in 2D detector systems. *Nucl. Instrum. Methods Phys. Res., Sect. A* **1994**, *346*, 312−321.

https://dx.doi.org/10.1021/acsomega.9b04501
ACS Omega 2020, 5, 9839−9845